# Magnetoelastic effects and spin excitations in $\gamma$-Mn alloys

R. S. Fishman
*Solid State Division, Oak Ridge National Laboratory, Oak Ridge, Tennessee 37831-6032*

S. H. Liu
*Physics Department, University of California, San Diego, California 92093*

(Received 31 August 1998)

A two-band model which includes the magnetoelastic interaction is used to study the magnetization and spin dynamics of $\gamma$-Mn alloys. As previously believed, single (S), double (D), and triple (T) spin-density wave (SDW) states are found in fct ($c<a$ and $c>a$) and fcc ($c=a$) lattices, respectively. When the magnetoelastic coupling constant $\kappa$ exceeds the critical value $\kappa_c$, both the structural and magnetic phase transitions become first order. This critical value drops to zero at the triple point, where the commensurate and incommensurate SDW phase boundaries meet. In agreement with experiments on fct MnNi and fcc FeMn alloys, we find that the gap $\Delta_{sw}(T)$ in the spin-wave dispersion is proportional to the 3/2 power of the sublattice magnetization $M(T)$. For the noncollinear D and T SDW magnetic phases observed in MnNi and FeMn alloys, we find an additional class of collective modes. This class includes a Goldstone mode which is produced by the modified dispersion of holes not directly involved in the SDW. We also find high-frequency excitations with energies of order $\Delta$, where $2\Delta \approx 2$ eV is the energy gap in the quasiparticle spectrum. Although these incoherent excitations have the same frequencies in the D and T SDW phases, their neutron-scattering cross sections should be 33% larger in the TSDW phase. [S0163-1829(99)05413-2]

## I. INTRODUCTION

Because the fcc phase of pure Mn is only stable between 1079 K and 1140 K, $\gamma$-Mn is commonly produced[1] by doping with Fe, Ni, or Cu. The importance of magnetoelastic effects in these alloys is demonstrated by the coincidence of the fcc to fct ($c<a$) structural phase transition with the Néel temperature of $Fe_xMn_{1-x}$ (Refs. 2 and 3) and $Mn_{1-x}Ni_x$ alloys[4] when $x<15\%$. More heavily doped $Fe_xMn_{1-x}$ ($x>45\%$[2]) and $Mn_{1-x}Ni_x$ ($x>22\%$) (Ref. 4) alloys remain cubic for all temperatures below $T_N$. In a narrow impurity range between 18% and 22%, MnNi alloys are fct at low temperatures with $c>a$. As indicated by the phase diagram in Fig. 1, an orthorombic phase joins the two tetragonal phases of MnNi alloys. Based on a phenomenological model, Jo and Hirai[5] demonstrated that these three crystal structures may be identified with the three magnetic phases sketched in Fig. 2. While the single (S) spin-density wave (SDW) phase is collinear, the noncollinear double (D) and triple (T) SDW phases are often grouped together as multiple (M) SDW's. Band-structure calculations[6,7] and experiments[8,9] have supported the presence of MSDW phases in MnNi and FeMn alloys. In this paper, we use a two-band Hamiltonian which includes the magnetoelastic interaction to study the spin dynamics of all three magnetic phases. For any magnetic phase, the gap $\Delta_{sw}(T)$ in the spin-wave (SW) spectrum is proportional to the 3/2 power of the sublattice magnetization $M(T)$. We also report a new class of incoherent spin excitations in the MSDW phases.

For low dopant concentrations, $\gamma$-Mn alloys have Néel temperatures close to 470 K and magnetic moments of about $2.3\mu_B$.[3] Both the magnetic moment and Néel temperature initially fall with the dopant concentration. At low temperatures, the tetragonality $t \equiv 1-c/a$ of fct MnNi,[4] MnCu,[10–12] and FeMn (Ref. 3) alloys varies from 3% to 5%. With increasing temperature, $t$ is proportional to $M(T)^2$ in MnCu alloys. While experiments initially suggested the presence of a pure SSDW in all such systems, Tsunoda and Nakai[13] discovered that the spin in MnCu alloys actually inclines about 5° from the $c$ axis. Recent measurements[14] have also revealed that the phase diagram of MnGa alloys is very similar to the MnNi phase diagram of Fig. 1, with DSDW and TSDW phases in tetragonal ($c>a$) and cubic phases. Because multiple domains of a SSDW or DSDW have the same neutron-scattering fingerprint as a TSDW,[2] Mössbauer transmission spectra[8] and $\gamma$-ray emission[9] have been used to detect the MSDW phases in FeMn and MnNi alloys.

Low-temperature energy gaps $\Delta_{sw}$ between 7 and 10 meV have been found in the excitation spectra of both fct (Refs. 15–19) and fcc (Refs. 20 and 21) Mn alloys. Early measure-

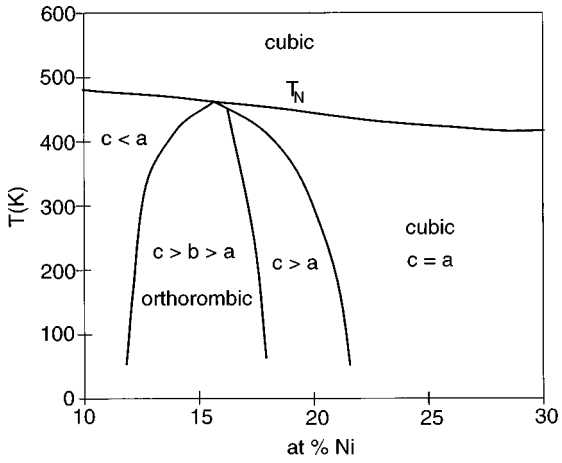


FIG. 1. The phase diagram of $Mn_{1-x}Ni_x$ alloys taken from Ref. 4.

 

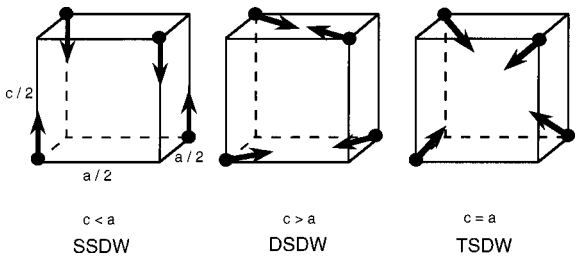


FIG. 2. The single, double, and triple SDW phases which are stabilized in different crystal structures.

ments by Tajima *et al.*[21] on fcc FeMn alloys reported that $\Delta_{sw}(T) \propto M(T)^{\alpha}$ with $\alpha = 3/2$. However, more recent measurements on fct MnNi (Ref. 22) and MnCu (Ref. 23) alloys have yielded power laws of 1.56 and 1.83, respectively. Until now, this temperature dependence has not been satisfactorily explained.

The commensurate SDW structures of Fig. 2 are produced by the Coulomb attraction $U$ between electrons on the electron Fermi surface $a$ centered at $\Gamma$ and holes on the six neighboring hole Fermi surfaces $b$ at the $X$ points.[24] For a fcc lattice, three distinct $X$ points correspond to each $\Gamma$, and so there are 3 times as many hole as electron Fermi surfaces. By contrast, the bcc lattice of Cr alloys supports one hole Fermi surface for every electron Fermi surface. Unlike the Fermi surfaces of Cr alloys,[25] the Fermi surfaces of $\gamma$-Mn alloys are so different in shape that only commensurate SDW ordering is possible. Below the Néel temperature, the Coulomb interaction $U$ produces electron-hole pairs with hybridized energies. The model described in the next section treats the magnetoelastic interaction within mean-field (MF) theory. Consequently, each electron or hole independently experiences the effective field $\mathbf{B}_i$ generated by the magnetoelastic interaction.

When the magnetoelastic constant $\kappa$ exceeds the critical value $\kappa_c$, the structural and magnetic phase transitions become first order, as observed in most $\gamma$-Mn alloys. Such a martensitic transformation[12] may be induced by the softening of a lattice phonon and the resulting enhancement of $\kappa$. The critical value $\kappa_c$ falls to zero as the mismatch between the electron and hole Fermi surfaces increases. At the triple point, where the commensurate phases of Fig. 2 become unstable to incommensurate phases, $\kappa_c$ vanishes and any nonzero magnetoelastic interaction will produce a first-order transition.

Our formalism for the spin dynamics combines a MF description of the magnetoelastic interaction together with an itinerant description of the $d$-band electrons. Close to the Néel transition, we find that $\Delta_{sw}(T) \propto \sqrt{\kappa T_N} M(T)^{\alpha}$ with $\alpha = 3/2$. By contrast, a power law of $\alpha = 2$ would be obtained from a local-moment description of $\gamma$-Mn based on a Heisenberg model with strain components proportional to $M(T)^2$. So the observation of a 3/2 power law implies that conduction-band electrons are responsible for the spin dynamics.

For a MSDW, only a fraction of the holes on each nested Fermi surface directly participate in the SDW. The energies of the remaining holes are unaltered by the SDW. A new class of collective excitations is produced by the Coulomb attraction between these unpaired holes and the paired electrons on the $a$ Fermi surface. These excitations include a Goldstone mode corresponding to the modified energy of an unpaired hole. Other excitations have frequencies of order $\Delta$, where $2\Delta \approx 2$ eV is the energy gap for the hybridized quasiparticle energies. One such high-frequency mode may have been observed in the fcc compound USb,[26] which is believed[27] to support a TSDW. Jensen and Bak[27] previously used the Heisenberg model to show that high-frequency excitations are permitted by the internal degrees of freedom of the TSDW structure.

We present our results in seven sections. Section II contains a discussion of our Hamiltonian and magnetoelastic effects. In Sec. III, we derive the Green's functions. The free energy is obtained in Sec. IV, followed by a derivation of the spin dynamics in Sec. V. Section VI presents our results and Sec. VII a discussion and conclusion. Details of our mathematical analysis are left to the three Appendixes. A short version of this work appeared in Ref. 28.

## II. HAMILTONIAN AND MAGNETOELASTIC ENERGIES

The S, D, and T SDW spin structures[29] of a fcc lattice may be written as

$$\mathbf{S}_i = M\hat{z}\cos(\mathbf{Q}_z \cdot \mathbf{R}_i), \tag{1a}$$

$$\mathbf{S}_i = \frac{1}{\sqrt{2}} M[\hat{x}\cos(\mathbf{Q}_x \cdot \mathbf{R}_i) + \hat{y}\cos(\mathbf{Q}_y \cdot \mathbf{R}_i)], \tag{1b}$$

$$\mathbf{S}_i = \frac{1}{\sqrt{3}} M[\hat{x}\cos(\mathbf{Q}_x \cdot \mathbf{R}_i) + \hat{y}\cos(\mathbf{Q}_y \cdot \mathbf{R}_i) + \hat{z}\cos(\mathbf{Q}_z \cdot \mathbf{R}_i)], \tag{1c}$$

where

$$\mathbf{Q}_x = 2\pi\hat{x}/a, \quad \mathbf{Q}_y = 2\pi\hat{y}/a, \quad \mathbf{Q}_z = 2\pi\hat{z}/c,$$

and

$$\cos(\mathbf{Q}_\gamma \cdot \mathbf{R}_i) = \pm 1.$$

To obtain Eqs. (1a)–(1c), the sharply peaked Bloch wave functions of the $d$-band electrons have been replaced by $\delta$ functions in the spin density. For the TSDW of Eq. (1c), the spin points along the $(1,1,1),(1,1,\overline{1}),(1,\overline{1},1)$, and $(\overline{1},1,1)$ directions. Consequently, a single domain of the TSDW phase does not violate cubic symmetry and is consistent with the cubic phase of FeMn and MnNi alloys. For a bcc lattice, $\mathbf{Q}_x$, $\mathbf{Q}_y$, and $\mathbf{Q}_z$ would all differ by a reciprocal lattice vector. So Eqs. (1a)–(1c) would reduce to the same collinear SDW state with different polarization directions.

Our Hamiltonian includes both the Coulomb attraction $U$ between quasiparticles on the $a$ and $b$ Fermi surfaces and the magnetoelastic interaction[10] between the $N$ spins and the lattice:

$$H = H_0 + H_{Coul} + H_{me}, \tag{2}$$

$$H_0 = \sum_{\mathbf{k},\alpha} \{\epsilon_a(\mathbf{k}) a^{\dagger}_{\mathbf{k}\alpha} a_{\mathbf{k}\alpha} + \epsilon_b(\mathbf{k}) b^{\dagger}_{\mathbf{k}\alpha} b_{\mathbf{k}\alpha}\}, \tag{3}$$

$$H_{Coul}=\frac{U}{V}\sum_{\mathbf{q},\mathbf{k},\mathbf{k}',\alpha,\beta} a^{\dagger}_{\mathbf{k}\alpha}b^{\dagger}_{\mathbf{k}'\beta}b_{\mathbf{k}'+\mathbf{q}\beta}a_{\mathbf{k}-\mathbf{q}\alpha}, \tag{4}$$

$$H_{me}=V\Big\{\frac{1}{2}c_{11}(\epsilon_{xx}^2+\epsilon_{yy}^2+\epsilon_{zz}^2)+c_{12}(\epsilon_{xx}\epsilon_{yy}+\epsilon_{yy}\epsilon_{zz}+\epsilon_{zz}\epsilon_{xx})$$
$$+\frac{g_1}{N}\sum_i (S_{ix}^2\epsilon_{xx}+S_{iy}^2\epsilon_{yy}+S_{iz}^2\epsilon_{zz})$$
$$+\frac{g_2}{N}(\epsilon_{xx}+\epsilon_{yy}+\epsilon_{zz})\sum_i (S_{ix}^2+S_{iy}^2+S_{iz}^2)\Big\}, \tag{5}$$

where $a^{\dagger}_{\mathbf{k}\alpha}$ and $b^{\dagger}_{\mathbf{k}\alpha}$ are the creation operators for electrons on the $a$ (electron) and $b$ (hole) bands. The strain components are given by $\epsilon_{ii}$, $c_{11}$ and $c_{12}$ are the elastic constants, and $g_i$ are the magnetoelastic coupling strengths. With terms up to order $S_{i\gamma}^2$, $H_{me}$ is the most general Hamiltonian consistent with the cubic symmetry of the paramagnetic phase. The final term in $H_{me}$ has the expectation value $g_2M^2\Delta V/V$ and produces the lowest-order effect of magnetostriction.

Missing from the Hamiltonian $H$ is the Coulomb interaction[30] between electrons and holes within the $a$ or $b$ Fermi surfaces. When sufficiently strong, this Coulomb interaction can generate a first-order transition even in the absence of magnetoelastic energies. But it is not needed to generate a SW gap.

After minimizing the Hamiltonian with respect to the strain components, it is easy to show that the average strain components for each SDW configuration are

$$\epsilon_{xx}=\epsilon_{yy}=M^2\frac{g_1c_{12}-g_2(c_{11}-c_{12})}{(c_{11}-c_{12})(c_{11}+2c_{12})},$$

$$\epsilon_{zz}=-M^2\frac{g_1(c_{11}+c_{12})+g_2(c_{11}-c_{12})}{(c_{11}-c_{12})(c_{11}+2c_{12})}\ \text{(SSDW)}, \tag{6a}$$

$$\epsilon_{xx}=\epsilon_{yy}=-\frac{1}{2}M^2\frac{g_1c_{11}+2g_2(c_{11}-c_{12})}{(c_{11}-c_{12})(c_{11}+2c_{12})},$$

$$\epsilon_{zz}=M^2\frac{g_1c_{12}-g_2(c_{11}-c_{12})}{(c_{11}-c_{12})(c_{11}+2c_{12})}\ \text{(DSDW)}, \tag{6b}$$

$$\epsilon_{xx}=\epsilon_{yy}=\epsilon_{zz}=-\frac{1}{3}M^2\frac{g_1+3g_2}{c_{11}+2c_{12}}\ \text{(TSDW)}. \tag{6c}$$

So in agreement with experiments,[10] the strain components are proportional to $M(T)^2$. The stability of the cubic crystal above $T_N$ requires that $c_{11}>0$, $c_{11}+2c_{12}>0$, $c_{11}-c_{12}>0$, and $c_{11}+c_{12}>0$.

The interaction constant $\kappa$ is defined in terms of $c_{11}$, $c_{12}$, and $g_i$ through the relation $\langle H_{me}\rangle=-N\kappa M^4$, which yields

$$\kappa=\kappa'+\frac{1}{2}\frac{V}{N}\frac{g_2(3g_2+2g_1)}{c_{11}+2c_{12}}, \tag{7}$$

where

$$\kappa'=\frac{1}{2}\frac{V}{N}g_1^2\frac{c_{11}+c_{12}}{(c_{11}-c_{12})(c_{11}+2c_{12})}\ \text{(SSDW)}, \tag{8a}$$

$$\kappa'=\frac{1}{4}\frac{V}{N}g_1^2\frac{c_{11}}{(c_{11}-c_{12})(c_{11}+2c_{12})}\ \text{(DSDW)}, \tag{8b}$$

$$\kappa'=\frac{1}{6}\frac{V}{N}g_1^2\frac{1}{c_{11}+2c_{12}}\ \text{(TSDW)}. \tag{8c}$$

Hence, the last term in $H_{me}$ with coefficient $g_2$ makes the same contribution to $\kappa$ for each SDW phase. The SDW contributions $\kappa'>0$ depend only on the coefficient $g_1$ and are independent of $g_2$.

For the S and D SDW's, the tetragonality $t=1-c/a=\epsilon_{xx}-\epsilon_{zz}$ is given by

$$t=g_1\frac{M^2}{c_{11}-c_{12}}\ \text{(SSDW)}, \tag{9a}$$

$$t=-\frac{g_1}{2}\frac{M^2}{c_{11}-c_{12}}\ \text{(DSDW)}, \tag{9b}$$

which are independent of $g_2$. The volume change below $T_N$ is the same in all three phases:

$$\frac{\Delta V}{V}=\epsilon_{xx}+\epsilon_{yy}+\epsilon_{zz}=-(g_1+3g_2)\frac{M^2}{c_{11}+2c_{12}}, \tag{10}$$

which implies that the final term in $H_{me}$ has the same expectation value in each magnetic phase. If $g_1>0$, then $t$ would be positive for a SSDW and negative for a DSDW, in agreement with the crystal structures identified by Jo and Hirai[5] in Fig. 2. The correspondence between the magnetic and crystal structures does not depend on the sign of $c_{12}$, which may be negative in some MnCu alloys.[12] A small value for $c_{11}-c_{12}$ would explain the large tetragonal distortion but the relatively modest volume contraction observed[4] in fct MnNi alloys. Indeed, Lowde *et al.*[31] have reported the softening of $c_{11}-c_{12}$ just above the martensitic transformation temperature of a MnNiC alloy.

The connection between the two tetragonal lattices and the magnetic phases sketched in Figs. 2(a) and 2(b) is physically obvious for a Heisenberg model with nearest-neighbor coupling. When $c=a$, the antiferromagnetic state of a fcc lattice is frustrated since two sets of nearest neighbors in the unit cell must be ferromagnetically aligned. This frustration is removed in the contracted lattice of Fig. 2(a), where nearest neighbors with opposite moments are separated by $\sqrt{a^2+c^2}/2<a/\sqrt{2}$. For the expanded lattice of Fig. 2(b), nearest-neighbor sites with opposite moments are separated by $a/\sqrt{2}<\sqrt{a^2+c^2}/2$.

Applying the MF approximation, we replace the magnetoelastic energy $H_{me}$ by

$$H'_{me}=-\sum_i \mathbf{B}_i\cdot\mathbf{S}_i+\text{const}, \tag{11}$$

with effective field components

$$B_{i\gamma}=-2\frac{V}{N}[g_1\epsilon_{\gamma\gamma}+g_2(\epsilon_{xx}+\epsilon_{yy}+\epsilon_{zz})]\langle S_{i\gamma}\rangle. \tag{12}$$

For each magnetic phase, $\mathbf{B}_i$ is parallel to $\langle\mathbf{S}_i\rangle$. Within this approximation, every electron and hole independently expe-

riences the effective field $\mathbf{B}_i$ exerted by the magnetoelastic interaction. The definition of $\mathbf{B}_i$ implies that the constant term in $H'_{me}$ is $3N\kappa M^4$.

### III. GREEN'S FUNCTIONS AND MANY-BODY THEORY

Using the standard notation, the imaginary time Green's functions may be written as

$$G(\mathbf{k},\tau)_{\alpha\beta,aa}=-\langle T_\tau a_{\mathbf{k}\alpha}(\tau)a^\dagger_{\mathbf{k}\beta}(0)\rangle=\delta_{\alpha\beta}G(\mathbf{k},\tau)_{aa}, \tag{13}$$

$$G(\mathbf{k},\tau)^\gamma_{\alpha\beta,bb}=-\langle T_\tau b_{\mathbf{k}+\mathbf{Q}_\gamma\alpha}(\tau)b^\dagger_{\mathbf{k}+\mathbf{Q}_\gamma\beta}(0)\rangle=\delta_{\alpha\beta}G(\mathbf{k},\tau)_{bb}, \tag{14}$$

$$G(\mathbf{k},\tau)^{\gamma\gamma'}_{\alpha\beta,bb'}=-\langle T_\tau b_{\mathbf{k}+\mathbf{Q}_\gamma\alpha}(\tau)b^\dagger_{\mathbf{k}+\mathbf{Q}_{\gamma'}\beta}(0)\rangle$$
$$=(\underline{\sigma}^\gamma\cdot\underline{\sigma}^{\gamma'})_{\alpha\beta}G(\mathbf{k},\tau)_{bb'}\quad\gamma\neq\gamma', \tag{15}$$

$$G(\mathbf{k},\tau)^\gamma_{\alpha\beta,ab}=-\langle T_\tau a_{\mathbf{k}\alpha}(\tau)b^\dagger_{\mathbf{k}+\mathbf{Q}_\gamma\beta}(0)\rangle=\sigma^\gamma_{\alpha\beta}G(\mathbf{k},\tau)_{ab}, \tag{16}$$

$$G(\mathbf{k},\tau)^\gamma_{\alpha\beta,ba}=-\langle T_\tau b_{\mathbf{k}+\mathbf{Q}_\gamma\alpha}(\tau)a^\dagger_{\mathbf{k}\beta}(0)\rangle=\sigma^\gamma_{\alpha\beta}G(\mathbf{k},\tau)_{ba}. \tag{17}$$

In Eqs. (14)–(17), $G(\mathbf{k},\tau)_{bb}$, $G(\mathbf{k},\tau)_{bb'}$, $G(\mathbf{k},\tau)_{ab}$, and $G(\mathbf{k},\tau)_{ba}$ are independent of $\gamma$ provided that the hole band $b$ has cubic symmetry about $X$ so that $\epsilon_b(\mathbf{k}+\mathbf{Q}_\gamma)\equiv\epsilon_{b+}(\mathbf{k})$ does not depend on $\gamma$. This approximation would be satisfied by spherical or octagonal Fermi surfaces. Notice that the Green's function is a four-, six-, or eight-dimensional matrix in band and spin space for the S, D, and T SDW phases.

In terms of the Fermi operators for the two bands, the spin operator is defined by

$$S_{i\gamma}=\frac{1}{2}(a^\dagger_{i\alpha}+b^\dagger_{i\alpha})\sigma^\gamma_{\alpha\beta}(a_{i\beta}+b_{i\beta}), \tag{18}$$

where repeated spin indices are summed and $\underline{\sigma}^\gamma$ are the Pauli matrices. Then using Eq. (16), the sublattice magnetization may be written

$$M=-\frac{2\sqrt{m}}{N}\sum_{\mathbf{k}}G(\mathbf{k},0^-)_{ab}=-\frac{2\sqrt{m}}{N}T\sum_{\mathbf{k},l}G(\mathbf{k},i\nu_l)_{ab}, \tag{19}$$

where $m=1$, 2, or 3 for S, D, and T SDW's. The above relation also introduces the Fourier-transformed Green's functions

$$G(\mathbf{k},i\nu_l)_{ij}=\int_0^\beta d\tau e^{i\nu_l\tau}G(\mathbf{k},\tau)_{ij}, \tag{20}$$

with Matsubara frequency $\nu_l=(2l+1)\pi T$.

A closed set of equations of motion for the Fourier-transformed Green's functions is obtained within the random-phase approximation (RPA):

$$[i\nu_l-\epsilon_a(\mathbf{k})]G(\mathbf{k},i\nu_l)_{aa}-m\Delta'G(\mathbf{k},i\nu_l)_{ab}=1, \tag{21}$$

$$[i\nu_l-\epsilon_{b+}(\mathbf{k})]G(\mathbf{k},i\nu_l)_{bb}-\Delta'G(\mathbf{k},i\nu_l)_{ab}=1, \tag{22}$$

$$[i\nu_l-\epsilon_{b+}(\mathbf{k})]G(\mathbf{k},i\nu_l)_{bb'}-\Delta'G(\mathbf{k},i\nu_l)_{ab}=0, \tag{23}$$

$$[i\nu_l-\epsilon_a(\mathbf{k})]G(\mathbf{k},i\nu_l)_{ab}-\Delta'G(\mathbf{k},i\nu_l)_{bb}$$
$$-(m-1)\Delta'G(\mathbf{k},i\nu_l)_{bb'}=0, \tag{24}$$

$$[i\nu_l-\epsilon_{b+}(\mathbf{k})]G(\mathbf{k},i\nu_l)_{ba}-\Delta'G(\mathbf{k},i\nu_l)_{aa}=0, \tag{25}$$

where

$$\Delta'=-\frac{U}{V}T\sum_{\mathbf{k},l}G(\mathbf{k},i\nu_l)_{ab}+\frac{2}{\sqrt{m}}\kappa M^3. \tag{26}$$

Since the reciprocal lattice is bcc, $\mathbf{Q}_x$, $\mathbf{Q}_y$, and $\mathbf{Q}_z$ are not related by reciprocal lattice vectors.

With $\Delta\equiv\sqrt{m}\Delta'$, the above relations are solved by

$$G(\mathbf{k},i\nu_l)_{aa}=\frac{i\nu_l-\epsilon_{b+}(\mathbf{k})}{D(\mathbf{k},i\nu_l)}, \tag{27}$$

$$G(\mathbf{k},i\nu_l)_{bb}=\frac{1}{m}\frac{i\nu_l-\epsilon_a(\mathbf{k})}{D(\mathbf{k},i\nu_l)}+\frac{m-1}{m}\frac{1}{i\nu_l-\epsilon_{b+}(\mathbf{k})}, \tag{28}$$

$$G(\mathbf{k},i\nu_l)_{bb'}=\frac{1}{m}\frac{i\nu_l-\epsilon_a(\mathbf{k})}{D(\mathbf{k},i\nu_l)}-\frac{1}{m}\frac{1}{i\nu_l-\epsilon_{b+}(\mathbf{k})}, \tag{29}$$

$$G(\mathbf{k},i\nu_l)_{ab}=G(\mathbf{k},i\nu_l)_{ba}=\frac{1}{\sqrt{m}}\frac{\Delta}{D(\mathbf{k},i\nu_l)}, \tag{30}$$

where

$$D(\mathbf{k},i\nu_l)=[i\nu_l-\epsilon_a(\mathbf{k})][i\nu_l-\epsilon_{b+}(\mathbf{k})]-\Delta^2. \tag{31}$$

Below the Néel temperature, the hybridized quasiparticle energies are obtained from the zeros of $D(\mathbf{k},\epsilon)$. So a gap of $2\Delta$ opens between the upper and lower hybridized bands. Notice that $\Delta(T)$ is enhanced by the magnetoelastic interaction. The energy gap $2\Delta$ may be inferred from the activation of the electrical resistivity or obtained directly from optical measurements. Unfortunately, neither set of measurements has been performed for $\gamma$-Mn alloys.

The physical significance of Eq. (28) for $G(\mathbf{k},i\nu_l)_{bb}$ is clear. For a MSDW, only $1/m$ of the holes on each of the $m$ nested hole Fermi surfaces (connected to each electron Fermi surface by the $m$ wave vectors $\mathbf{Q}_\gamma$) participates in the SDW and experiences an energy gap. The remaining fraction $1-1/m$ of the holes are unaffected by the formation of the SDW.

In all three magnetic phases, the quasiparticle energy gap $\Delta$ is given by

$$\Delta(T)=\frac{N}{2V}UM(T)+2\kappa M(T)^3, \tag{32}$$

where $UN/V$ has units of energy. The magnetization is also formally identical in all three phases:

$$M(T)=-\frac{2}{N}T\sum_{\mathbf{k},l}\frac{\Delta}{D(\mathbf{k},i\nu_l)}. \tag{33}$$

However, recall that Eqs. (8a)–(8c) for $\kappa'$ in terms of $g_1$, $c_{11}$, and $c_{12}$ are different in the three magnetic phases.

Because of the size difference between the electron and hole Fermi surfaces, there is an energy mismatch $\epsilon_{b+}(\mathbf{k})$

$-\epsilon_a(\mathbf{k})=z_0/2$ at the Fermi momentum $\mathbf{k}_F$ of the $a$ Fermi surface. Assuming this mismatch to be the same for all points on the $a$ Fermi surface, momentum summations over $\mathbf{k}$ may be evaluated with the linearized energies $\epsilon_a(\mathbf{k})\equiv z$ and $\epsilon_{b+}(\mathbf{k})\equiv z_0/2-z$.

Using Eq. (33) and the linearized quasiparticle energies, the self-consistent equation for the energy gap may be written as

$$\frac{1}{U+4\kappa M^2V/N}=-\frac{1}{4}\pi i T\rho_{eh}\sum_l \frac{1}{x_l}\mathrm{sgn}(\nu_l), \tag{34}$$

$$x_l=\sqrt{(z_0/2-2i\nu_l)^2-4\Delta^2}, \tag{35}$$

where $\rho_{eh}$ is the two-spin density of states for the one-electron and three-hole Fermi surfaces. So the density of states for a pair of nested electron and hole Fermi surfaces is $\rho_{eh}/2$.[32] The complex function $x_l$ is defined so that $\mathrm{sgn}[\mathrm{Im}(x_l)]=-\mathrm{sgn}(\nu_l)$. Because the sum on the right-hand side of Eq. (34) is formally divergent, it must be cut off at frequencies $\nu_l=\pm\epsilon_0$. The cutoff $\epsilon_0$ has precisely the same significance as in BCS theory: quasiparticles are only defined within the range $\pm\epsilon_0$ of the Fermi energy $\epsilon_F$. Although undetermined within BCS theory and within our model, $\epsilon_0$ is subject to the restrictions $T\ll\epsilon_0\ll\epsilon_F$.

Solving Eq. (34) with $z_0=0$ as $M\to 0$, we find that the Néel temperature of a perfectly nested alloy is given by

$$T_{\mathrm{N}}^{\star}=\frac{2\gamma}{\pi}\epsilon_0 e^{-8/U\rho_{eh}}, \tag{36}$$

where $\ln\gamma\approx 0.577$ is Euler's constant. Since the nesting between the two Fermi surfaces is imperfect with $z_0\neq 0$, the actual Néel temperature $T_{\mathrm{N}}$ will be much less than $T_{\mathrm{N}}^{\star}$. When $\kappa=0$ and $T=0$, Eq. (34) yields the quasiparticle gap $\Delta(0)=\pi T_{\mathrm{N}}^{\star}/\gamma$, which is identical to the familiar BCS relation for the energy gap of a superconductor. When $\kappa>0$, the zero-temperature gap is given by

$$\Delta(0)=\frac{\pi}{\gamma}T_{\mathrm{N}}^{\star}\exp[4\phi(0)^2], \tag{37}$$

where

$$\phi(T)=\sqrt{\frac{4\kappa M(T)^2}{NU/V+4\kappa M(T)^2}\frac{2}{\rho_{eh}U}}\approx\frac{2M(T)}{U}\sqrt{\frac{2\kappa V}{N\rho_{eh}}} \tag{38}$$

is proportional to $M(T)\sqrt{\kappa/T_{\mathrm{N}}^{\star}}$. Since $\phi(0)\ll 1$, $\Delta(0)$ is slightly enhanced by the magnetoelastic interaction.

At zero temperature, Eq. (37) must be solved simultaneously with Eq. (32) for $\Delta(0)$ in terms of $M(0)$. Physically reasonable solutions are obtained for small values of $\kappa$. Because Eq. (37) is independent of the energy mismatch $z_0$ and $\phi(0)\ll 1$, $2\Delta(0)$ should be the same for any $\gamma$-Mn alloy.

In the absence of optical measurements, it is difficult to estimate either $2\Delta(0)$ or $T_{\mathrm{N}}^{\star}$ for $\gamma$-Mn alloys. Based on band-structure calculations, Asano and Yamashita[33] suggested that $2\Delta(0)$ lies between 1.8 and 2.2 eV, corresponding to an ideal Néel temperature $T_{\mathrm{N}}^{\star}$ between 500 and 600 meV.[34] Then the stability of the commensurate SDW structures sketched in Fig. 2 requires that the energy mismatch $z_0$ be less than $4\Delta(0)\approx 4$ eV. All of these parameters are still smaller than the $d$-band width of about 5.5 eV.[33]

## IV. FREE ENERGY AND LANDAU-GINZBURG EXPANSION

The derivation of the free energy for $\gamma$-Mn alloys follows the same steps as for Cr alloys,[35] except that we must explicitly include the magnetoelastic constant term in Eq. (11). In terms of the magnetization $M$, the free energy difference between the magnetic and paramagnetic phases is given by

$$\Delta F=\frac{N}{V}\left\{\frac{NU}{2V}M^2+3\kappa M^4-\frac{2T}{N}\sum_{\mathbf{k},l}\ln\left|\frac{D(M,\mathbf{k},i\nu_l)}{D(0,\mathbf{k},i\nu_l)}\right|\right\}, \tag{39}$$

where Eq. (32) is used to replace $\Delta$ by $M$ in $D(\mathbf{k},i\nu_l)$. Minimizing this free energy with respect to $M$ reproduces Eq. (33).

To obtain the Landau-Ginzburg expansion of the free energy in powers of $M$, we perform the momentum summations with the aid of the linearized quasiparticle energies defined above:

$$\frac{V}{N}\frac{\Delta F}{T_{\mathrm{N}}^{\star}}=AM^2+BM^4+CM^6+\cdots, \tag{40}$$

with quadratic and quartic coefficients

$$A=\frac{NU^2}{16VT_{\mathrm{N}}^{\star}}\rho_{eh}\left\{\ln\left(\frac{T}{T_{\mathrm{N}}^{\star}}\right)-\sum_{n=0}^{\infty}\left[\mathrm{Re}\left(\frac{1}{X_n}\right)-\frac{1}{n+1/2}\right]\right\}, \tag{41}$$

$$B=-\frac{\kappa}{T_{\mathrm{N}}^{\star}}+8A\frac{V\kappa}{NU}+\frac{N^3U^4}{1024\pi^2V^3T_{\mathrm{N}}^{\star}T^2}\rho_{eh}S_3, \tag{42}$$

where $X_n=n+1/2+iz_0/8\pi T$ and

$$S_3(z_0/T)=\sum_{n=0}^{\infty}\mathrm{Re}\left(\frac{1}{X_n^3}\right). \tag{43}$$

A first-order phase transition requires that $A>0$ and $B<0$. So the coupled structural and magnetic phase transition becomes first order when $\kappa>\kappa_c$, where

$$\kappa_c=\frac{N^3U^4}{1024\pi^2V^3T_{\mathrm{N}}^2}\rho_{eh}S_3(z_0/T_{\mathrm{N}}). \tag{44}$$

The summation $S_3(z_0/T_{\mathrm{N}})$ is a monotonically decreasing function of the energy mismatch $z_0$. At the triple point $z_0=4.2913T_{\mathrm{N}}^{\star}$, where the commensurate SDW structures of Fig. 2 become unstable to an incommensurate SDW phase at $T_{\mathrm{N}}$, both $S_3$ and $\kappa_c$ vanish. So any small magnetoelastic interaction will produce a first-order phase transition at the triple point. When $\kappa>\kappa_c$, the first-order Néel temperature $T_{\mathrm{N}}^{(1)}$ is solved from the condition $B^2-4AC=0$.

For a given $\kappa$ and $z_0$, all three magnetic phases have the same free energy. But for a fixed set of elastic constants $\{c_{11},c_{12},g_1,g_2\}$, $\kappa$ is different in the S, D, and T SDW phases. Then the magnetic phase with the largest $\kappa$ has the

lowest free energy. The question of which magnetic phase is stable for a given set of material parameters will be briefly addressed in the final section. Until then, we shall separately examine the spin dynamics of each magnetic phase.

## V. SPIN DYNAMICS

Collective spin excitations are obtained from the poles of the spin correlation function

$$\chi_{\alpha\beta}(\mathbf{q},\omega)=\int_0^\beta d\tau e^{i\omega_n\tau}\langle T_\tau S(\mathbf{q},\tau)_\beta S(-\mathbf{q},0)_\alpha\rangle|_{i\omega_n\to\omega+i\varepsilon^+}, \tag{45}$$

where $\mathbf{S}(\mathbf{q})$ is the Fourier transform of the spin operator in Eq. (18). We also define the specific Matsubara correlation functions

$$\chi_1^{\gamma_1\gamma_2}(\mathbf{q},i\omega_n)=\frac{1}{V}\sum_{\mathbf{k},\mathbf{k}'}\int_0^\beta d\tau e^{i\omega_n\tau}\langle T_\tau b^\dagger_{\mathbf{k}+\mathbf{q}+\mathbf{Q}_{\gamma_1},\uparrow}(\tau)\times a_{\mathbf{k},\uparrow}(\tau)a^\dagger_{\mathbf{k}',\uparrow}(0)b_{\mathbf{k}'+\mathbf{q}+\mathbf{Q}_{\gamma_2},\uparrow}(0)\rangle, \tag{46}$$

$$\overline{\chi}_1^{\gamma_1\gamma_2}(\mathbf{q},i\omega_n)=\frac{1}{V}\sum_{\mathbf{k},\mathbf{k}'}\int_0^\beta d\tau e^{i\omega_n\tau}\langle T_\tau a^\dagger_{\mathbf{k}+\mathbf{q},\uparrow}(\tau)b_{\mathbf{k}+\mathbf{Q}_{\gamma_1},\uparrow}(\tau)\times b^\dagger_{\mathbf{k}'+\mathbf{Q}_{\gamma_2},\uparrow}(0)a_{\mathbf{k}'+\mathbf{q},\uparrow}(0)\rangle, \tag{47}$$

$$\chi_2^{\gamma_1\gamma_2}(\mathbf{q},i\omega_n)=\frac{1}{V}\sum_{\mathbf{k},\mathbf{k}'}\int_0^\beta d\tau e^{i\omega_n\tau}\langle T_\tau a^\dagger_{\mathbf{k}+\mathbf{q},\uparrow}(\tau)b_{\mathbf{k}+\mathbf{Q}_{\gamma_1},\uparrow}(\tau)\times a^\dagger_{\mathbf{k}',\uparrow}(0)b_{\mathbf{k}'+\mathbf{q}+\mathbf{Q}_{\gamma_2},\uparrow}(0)\rangle, \tag{48}$$

$$\overline{\chi}_2^{\gamma_1\gamma_2}(\mathbf{q},i\omega_n)=\frac{1}{V}\sum_{\mathbf{k},\mathbf{k}'}\int_0^\beta d\tau e^{i\omega_n\tau}\langle T_\tau b^\dagger_{\mathbf{k}+\mathbf{q}+\mathbf{Q}_{\gamma_1},\uparrow}(\tau)a_{\mathbf{k},\uparrow}(\tau)\times b^\dagger_{\mathbf{k}'+\mathbf{Q}_{\gamma_2},\uparrow}(0)a_{\mathbf{k}'+\mathbf{q},\uparrow}(0)\rangle, \tag{49}$$

where $\omega_n=2n\pi T$. These correlation functions are represented graphically by the circles in Fig. 3.

Transverse and longitudinal spin excitations are now evaluated about one of the ordering wave vectors $\mathbf{Q}_\gamma$. With respect to the spin quantization axis $\hat{\mathbf{r}}_\gamma$, the transverse and longitudinal susceptibilities are

$$\chi_t(\mathbf{q},\omega)=2[\chi_1^{\gamma\gamma}(\mathbf{q},\omega)+\overline{\chi}_1^{\gamma\gamma}(\mathbf{q},\omega)-\chi_2^{\gamma\gamma}(\mathbf{q},\omega)-\overline{\chi}_2^{\gamma\gamma}(\mathbf{q},\omega)], \tag{50}$$

$$\chi_l(\mathbf{q},\omega)=\chi_1^{\gamma\gamma}(\mathbf{q},\omega)+\overline{\chi}_1^{\gamma\gamma}(\mathbf{q},\omega)+\chi_2^{\gamma\gamma}(\mathbf{q},\omega)+\overline{\chi}_2^{\gamma\gamma}(\mathbf{q},\omega), \tag{51}$$

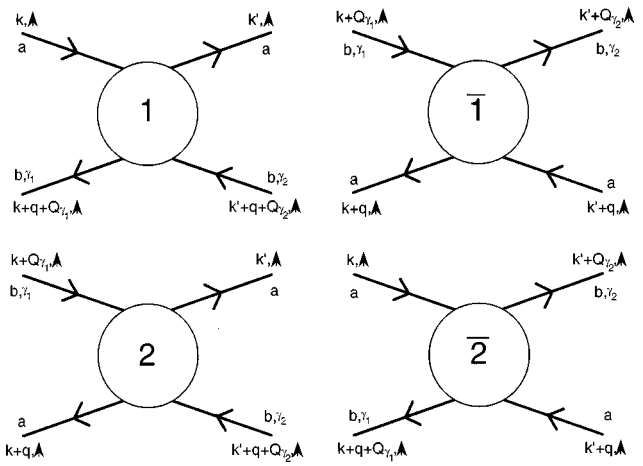


FIG. 3. A graphical representation of the correlation functions in Eqs. (46)–(49).

where only the band-diagonal correlation functions $\chi_i^{\gamma\gamma}(\mathbf{q},\omega)=\chi_i^{\gamma\gamma}(\mathbf{q},i\omega_n\to\omega+i\varepsilon^+)$ appear in order to guarantee momentum conservation. Throughout the rest of this section, the wave vector difference $|\mathbf{q}-\mathbf{Q}_\gamma|$ is assumed to be much smaller than the Fermi momentum $k_F$.

The RPA for the spin correlation functions is quite similar in all three SDW phases, except that the correlation functions with different $\mathbf{Q}_\gamma$ are coupled to the band-diagonal terms in the MSDW phases. By symmetry considerations, $\chi_i(\mathbf{q},\omega)\equiv\chi_i^{\gamma\gamma}(\mathbf{q},\omega)$ are independent of $\gamma$. Similarly, the off-diagonal correlation functions $\chi_i'(\mathbf{q},\omega)=\chi_i^{\gamma_1\gamma_2}(\mathbf{q},\omega)$ with $\gamma_1\neq\gamma_2$ are independent of $\gamma_1$ and $\gamma_2$. The resulting RPA equations for the correlation functions are sketched in Fig. 4 and listed in Appendix A. The Hartree-Fock (HF) correlation functions $\chi_i^{(0)}(\mathbf{q},\omega)$ and $\overline{\chi}_i^{(0)}(\mathbf{q},\omega)$ are evaluated with $U=0$ and are represented by squares in Fig. 4.

Upon solving the coupled equations, we obtain the transverse and longitudinal susceptibilities in terms of the HF correlation functions:

$$\chi_t=\frac{2}{U}\left\{-2+\frac{m-1}{m}\left(\frac{1}{1-U\chi_4^{(0)}}+\frac{1}{1-U\overline{\chi}_4^{(0)}}\right)+\frac{1}{m}\left(\frac{1}{1-U(\chi_3^{(0)}-m\chi_2^{(0)})}+\frac{1}{1-U(\overline{\chi}_3^{(0)}-m\chi_2^{(0)})}\right)\right\}, \tag{52}$$

$$\chi_l=\frac{1}{U}\left\{-2+\frac{m-1}{m}\left(\frac{1}{1-U\chi_4^{(0)}}+\frac{1}{1-U\overline{\chi}_4^{(0)}}\right)+\frac{1}{m}\left(\frac{1}{1-U(\chi_3^{(0)}+m\chi_2^{(0)})}+\frac{1}{1-U(\overline{\chi}_3^{(0)}+m\chi_2^{(0)})}\right)\right\}, \tag{53}$$

where $\chi_3^{(0)}$ and $\chi_4^{(0)}$ are defined by Eqs. (A10) and (A11). The transverse and longitudinal excitations of all three phases can be evaluated from the zeros of $F_\pm(\mathbf{q},\omega)=1-U[\chi_3^{(0)}(\mathbf{q},\omega)\pm m\chi_2^{(0)}(\mathbf{q},\omega)]$. Using the results in Appendix B, it can be shown that $\overline{F}_\pm(\mathbf{q},\omega)=F_\pm(\mathbf{q},\omega)$ so that no

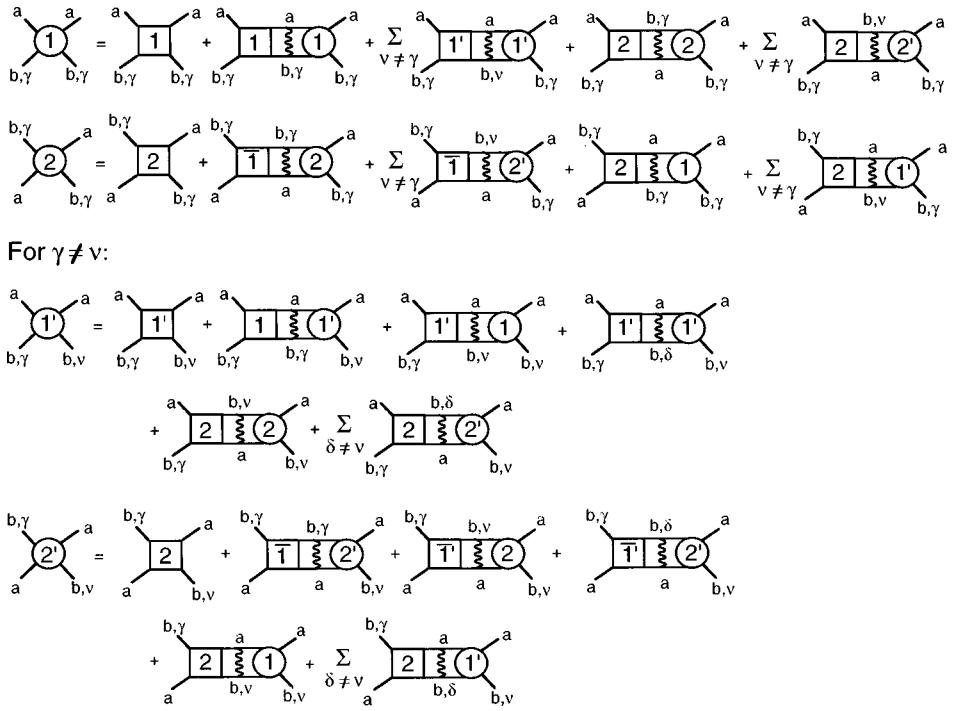


FIG. 4. The RPA equations for the spin correlation functions, with $U$ represented by wiggly lines.

additional zeros are introduced by the terms with an overbar. Notice that MSDW's with $m>1$ support an additional class of collective excitations given by the zeros of $F_{\rm i}(\mathbf{q},\omega)=1-U\chi_4^{(0)}(\mathbf{q},\omega)$ and $\overline{F}_{\rm i}(\mathbf{q},\omega)=F_{\rm i}(\mathbf{q},-\omega)^*$.[36]

It follows from Eqs. (30) and (A9) that $m\chi_2^{(0)}(\mathbf{q},\omega)$ is identical in all three magnetic phases. Therefore, the longitudinal and transverse mode frequencies, which are obtained by solving the conditions $F_{\pm}(\mathbf{q},\omega)=0$, are the same in the S, D, and T SDW phases.

From Eqs. (A10) and (A11), we find that $F_{\pm}(\mathbf{q},\omega)$ for the D and T SDW states involves the linear combinations of operators $b_{\mathbf{k}+\mathbf{Q}_{\gamma_1},\alpha}+b_{\mathbf{k}+\mathbf{Q}_{\gamma_2},\alpha}$ or $b_{\mathbf{k}+\mathbf{Q}_{\gamma_1},\alpha}+b_{\mathbf{k}+\mathbf{Q}_{\gamma_2},\alpha}+b_{\mathbf{k}+\mathbf{Q}_{\gamma_3},\alpha}$, respectively. By contrast, $F_{\rm i}(\mathbf{q},\omega)$ and $\overline{F}_{\rm i}(\mathbf{q},\omega)$ involve the linear combinations $b_{\mathbf{k}+\mathbf{Q}_{\gamma_1},\alpha}-b_{\mathbf{k}+\mathbf{Q}_{\gamma_2},\alpha}$ (DSDW) or $2b_{\mathbf{k}+\mathbf{Q}_{\gamma_1},\alpha}-b_{\mathbf{k}+\mathbf{Q}_{\gamma_2},\alpha}-b_{\mathbf{k}+\mathbf{Q}_{\gamma_3},\alpha}$ (TSDW). Consequently, the quasiparticles on the $m$ nested hole Fermi surfaces contribute incoherently. Like the transverse and longitudinal mode frequencies, the incoherent mode frequencies are identical in the D and T SDW states.

The HF susceptibilities defined in Appendix A and summarized in Appendix B are evaluated by the same techniques described in our previous work[37] on the commensurate spin dynamics of Cr alloys. However, the HF susceptibilities of $\gamma$-Mn now include additional contributions when $\mathbf{Q}_\gamma \neq \mathbf{Q}_{\gamma'}$. Other new features in the HF susceptibilities can be traced to the modified self-consistent relation for $\Delta$. In the next section, we show that the $\kappa M^2$ term in Eq. (34) is responsible for the gap in the SW excitation spectrum.

## VI. COLLECTIVE MODES

In the next three subsections, we shall separately discuss our results for the SW, amplitude, and incoherent collective modes. The division of these excitations into purely transverse or longitudinal modes is somewhat tricky because the spin quantization axis depends on the magnetic satellite. For example, transverse excitations about $\mathbf{Q}_x$ involve spin flips from $+\hat{x}$ to $-\hat{x}$. Such spin flips will couple to both the transverse and longitudinal excitations about $\mathbf{Q}_y$.

### A. Spin-wave modes

The SW excitations are obtained from the zeros of $F_-(\mathbf{q},\omega)$. Because the magnetoelastic interaction violates rotational symmetry, the SW spectrum contains an energy gap $\Delta_{\rm sw}(T)$, which is formally the same in all three magnetic phases.

For $T=0$, the SW gap derived in Appendix C may be written as $\Delta_{\rm sw}(0)=4\Delta(0)\phi(0)$, where $\phi(T)$ was defined by Eq. (38). Since $\phi(0)\ll 1$, $\Delta_{\rm sw}(0)$ is much smaller than the zero-temperature energy gap $\Delta(0)$.

In a SSDW, the SW gap is produced by the lattice contraction along the $c$ axis. This contraction generates an effective field $\mathbf{B}_i$ which violates rotational symmetry. For a DSDW, the expansion along the $c$ axis creates local, effective fields $\mathbf{B}_i$ in the $ab$ plane which once again violate rotational symmetry. At first sight, the presence of a SW gap in cubic FeMn alloys is harder to understand, since the TSDW state preserves the cubic symmetry of the lattice with $\epsilon_{xx}=\epsilon_{yy}=\epsilon_{zz}<0$. But as in the other two SDW phases, the SW gap is produced by the effective field $\mathbf{B}_i$ experienced by the spin on each lattice site of the strained lattice. Although it maintains the cubic symmetry of the TSDW phase, this effective field still destroys the rotational invariance of the Hamiltonian.

For small $\phi(T)$, the SW dispersion may be closely approximated by $\omega_{\rm sw}(\mathbf{q})=\sqrt{\Delta_{\rm sw}(T)^2+(cq)^2}$, where the SW velocity $c$ is proportional to the Fermi velocity. This form for

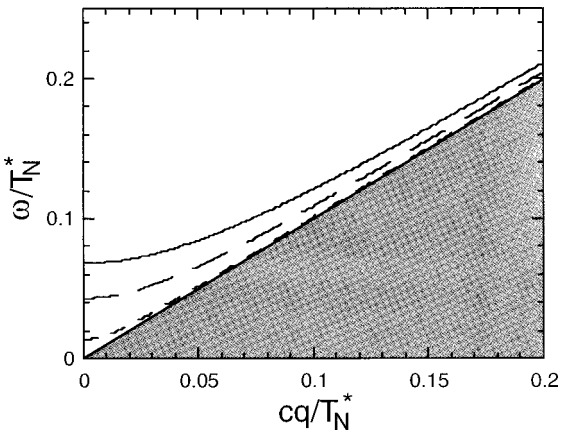


FIG. 5. The SW dispersion with $UN/V=3.068T_{\mathrm{N}}^{\star}$, $\rho_{eh}VT_{\mathrm{N}}^{\star}/N=0.3, z_0=4.29T_{\mathrm{N}}^{\star}$, and $\kappa/T_{\mathrm{N}}^{\star}=2.5\times10^{-5}$ (solid line), $1.0\times10^{-5}$ (long dashed line), and $1.0\times10^{-6}$ (short dashed line) at $T/T_{\mathrm{N}}=0.1$. The shaded region contains single-particle excitations.

$\omega_{\mathrm{sw}}(\mathbf{q})$ was found[17] to be satisfied by a $Mn_{90}Cu_{10}$ alloy up to about 190 meV. The precise value of $c$ depends on the Fermi surface topology and on the angle between $\mathbf{q}$ and $\mathbf{Q}_{\gamma}$ but is otherwise independent of the magnetic phase. For octagonal or spherical Fermi surfaces with $\mathbf{q}$ parallel to $\mathbf{Q}_{\gamma}$, $c=v_F/\sqrt{3}$. In fct MnFe,[15] MnCu,[16–18] and MnGe (Ref. 19) alloys, the observed SW velocities range from 180 to 250 meV Å . SW velocities of similar sizes were observed[20,21] in fcc MnFe alloys. Unfortunately, there are no good estimates for the Fermi velocity of any $\gamma$-Mn alloy due to the large effective mass. So we cannot compare the measured value of $c/v_F$ with the predictions of our model.

In Fig. 5, the SW dispersion is plotted for three values of $\kappa$ when $T/T_{\mathrm{N}}=0.1$. Both $\omega$ and $cq$ are scaled by the Néel temperature $T_{\mathrm{N}}^{\star}$ of a perfectly nested alloy with $z_0=0$. The value for the density of states used in this figure follows from the band-structure calculations of Asano and Yamashita.[33] Other parameters were chosen to produce a magnetic moment of $2.3\mu_{\mathrm{B}}$ and a critical value of $\kappa_c=0$. The largest value of $\kappa$ corresponds to an effective field $|\mathbf{B}_i|$ of about 0.32 T while the smallest corresponds to an effective field 25 times smaller. If $\Delta_{\mathrm{sw}}\approx10$ meV and $T_{\mathrm{N}}^{\star}\approx0.5$ eV, we estimate that $\kappa\approx0.75$ $\mu$ eV and $|\mathbf{B}_i|\approx200$ G.

Single-particle excitations occupy the shaded portion of Fig. 5 and also lie above the Stoner pair-breaking threshold at $\omega_{\mathrm{pb}}=\sqrt{4\Delta^2+(cq)^2}$. So the SW modes are undamped within the RPA. Experimentally, the SW modes are damped with a width proportional to the wave vector $q$.[16,21] This damping may be produced either by impurity scattering or by the decay of SW's into single-particle excitations[38] of the nongapped portions of the Fermi surface.

The temperature dependence of the SW gap is plotted in Fig. 6 using the same parameters as in Fig. 5. Over a wide range of temperatures, $\Delta_{\mathrm{sw}}(T)$ is approximately proportional to $M(T)^{3/2}$, as shown in Fig. 7. In both Figs. 6 and 7, $T_N^{(2)}$ is the second-order Néel temperature, which is exceeded when $\kappa>\kappa_c$. Only a modest decrease in $\Delta_{\mathrm{sw}}(T)/M(T)^{3/2}$ occurs close to $T_N^{(1)}$. The temperature variation in $\Delta_{\mathrm{sw}}(T)/M(T)^{3/2}$ increases as $\kappa$ becomes larger.

For small values of $M(T)$ close to the Néel temperature, Appendix B shows that

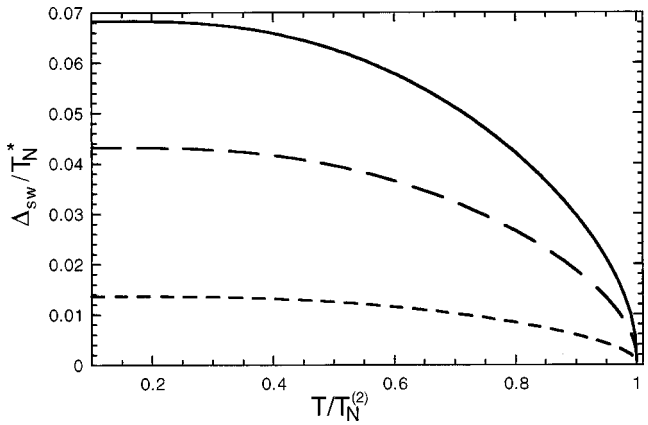


FIG. 6. The normalized SW gap $\Delta_{\mathrm{sw}}(T)/T_{\mathrm{N}}^{\star}$ vs temperature for the same parameters as in Fig. 5.

$$\Delta_{\mathrm{sw}}(T)=\frac{16}{\sqrt{\pi}}\sqrt{\frac{\kappa T_{\mathrm{N}}}{\rho_{eh}U}}\cosh\left(\frac{z_0}{8T_{\mathrm{N}}}\right)M(T)^{3/2}. \tag{54}$$

Consequently, the SW gap is proportional to the $\alpha=3/2$ power of the sublattice magnetization and grows with the mismatch $z_0$ between the Fermi surfaces.

A power law with $\alpha=2$ would be obtained from a local-moment description of $\gamma$-Mn based on the Heisenberg model, provided that the strain components $\epsilon_{ii}$ are proportional to $M^2$. By contrast, Sato and Maki[39] used a two-band RPA to predict that $\alpha=1$, which would follow from a Heisenberg model with temperature-independent strain.[40] A power law of $\alpha=3/2$ only arises from an approach such as ours, which combines a local treatment of the magnetoelastic interaction together with an itinerant description of the electronic response.

While Tajima *et al.*[21] observed a 3/2 power dependence for three different fcc FeMn alloys, more recent studies of fct MnCu (Ref. 22) and MnNi (Ref. 23) alloys find power laws with $\alpha=1.56$ and 1.83, respectively. But the statistics of the latter study are not convincing.

### B. Amplitude modes

Next we turn to the longitudinal excitations, which correspond to oscillations in the SDW amplitude $M(T)$. When

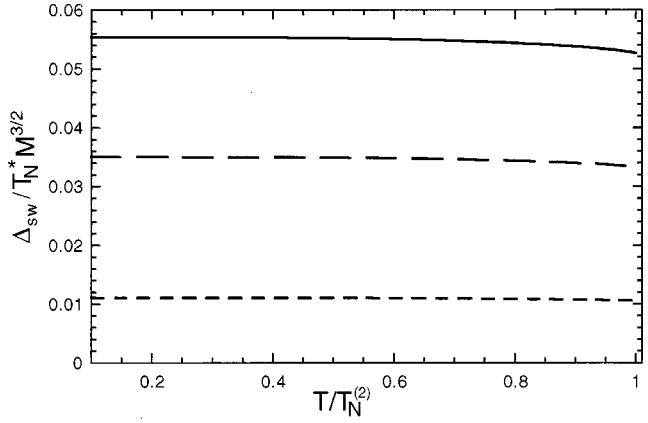


FIG. 7. The dimensionless ratio $\Delta_{\mathrm{sw}}(T)/T_{\mathrm{N}}^{\star}M(T)^{3/2}$ vs temperature for the same parameters as in Fig. 5.

$\kappa=0$, the zeros of the denominator $F_+(\mathbf{q},\omega)$ coincide with the pair-breaking edge $\omega_{\rm pb}=\sqrt{4\Delta^2+(cq)^2}$. Recall that damped excitations decay in time exponentially with a time scale inversely proportional to the imaginary part of the denominator. Although the amplitude modes are undamped, they are not associated with delta functions in $1/F_+(\mathbf{q},\omega)$ due to the behavior of the real and imaginary parts of $F_+(\mathbf{q},\omega)$ near its zeros (see the discussion in Ref. 37). Therefore, oscillations of the SDW amplitude $M(T)$ decay in time according to a power law, just as in commensurate Cr alloys,[37] and the amplitude modes are marginal excitations when $\kappa=0$.

When $\kappa>0$, the real part of $F_+(\mathbf{q},\omega)$ no longer vanishes at any frequency or wave vector. Hence, the amplitude modes are overdamped by the magnetoelastic coupling. Since the effective field $\mathbf{B}_i$ directly couples to the SDW amplitude, this result is not surprising.

### C. Incoherent collective modes

The incoherent excitations appear as peaks in $1/F_{\rm i}(\mathbf{q},\omega)$ or $1/\overline{F}_{\rm i}(\mathbf{q},\omega)=1/F_{\rm i}(\mathbf{q},-\omega)^*$ where $F_{\rm i}(\mathbf{q},\omega)=F_{\rm i}^{(1)}(\mathbf{q},\omega)+iF_{\rm i}^{(2)}(\mathbf{q},\omega)$. As seen from Eqs. (52), (53), and (A11), incoherent modes arise from the Coulomb attraction between the fraction $1/m$ of unpaired holes on the $m$ nested $b$ Fermi surfaces with the paired electrons on the $a$ Fermi surface. So these excitations are not related to the magnetoelastic interactions. Because the unpaired holes do not experience an energy gap, $F_{\rm i}^{(2)}(\mathbf{q},\omega)$ given by Eq. (C2) never vanishes and the damped, incoherent excitations are fixed by the condition $F_{\rm i}^{(1)}(\mathbf{q},\omega)=0$.

For $T=0$ and $\mathbf{q}=0$, the incoherent mode frequencies with $\omega>0$ are summarized by Eqs. (C4)–(C7). When $z_0=0$, $\omega_{\rm i}^{(1)}(\mathbf{q}=0)=\omega_{\rm i}^{(2)}(\mathbf{q}=0)\approx 2\sqrt{2}\phi(0)\Delta(0)$ and $\omega_{\rm i}^{(3)}(0)=\omega_{\rm i}^{(4)}(0)\approx\sqrt{2}\Delta(0)$, which use the fact that $\phi(0)\ll 1$. Hence, $\omega_{\rm i}^{(1)}(0)=\omega_{\rm i}^{(2)}(0)\approx\Delta_{\rm sw}(0)/\sqrt{2}$ both lie below the SW gap. For $z_0\gg 8\sqrt{2}\Delta(0)\phi(0)$, as expected for a realistic alloy, $\omega_{\rm i}^{(1)}(0)\approx\Delta_{\rm sw}(0)^2/z_0$ and $\omega_{\rm i}^{(2)}(0)\approx z_0/2$. Since $\omega_{\rm i}^{(1)}(0)/\Delta_{\rm sw}(0)\approx\Delta_{\rm sw}(0)/z_0\ll 1$ this excitation has a very low energy of order 1 meV or less. Also for $z_0>0$, the third and fourth modes split away from $\sqrt{2}\Delta(0)$.

Unlike the SW gap, $\omega_{\rm i}(T,\mathbf{q}=0)$ all fall in temperature according to an integer power of $M(T)$. It can be shown analytically that $\omega_{\rm i}^{(1)}(T,0)$ and $\omega_{\rm i}^{(2)}(T,0)$ fall off like $M(T)^2$ while $\omega_{\rm i}^{(3)}(T,0)$ and $\omega_{\rm i}^{(4)}(T,0)$ decrease like $M(T)$.

The results of Appendix C were used to plot the dispersion of the incoherent modes in Figs. 8 and 9. Due to their high frequencies, the incoherent mode frequencies plotted in Fig. 8 depend very weakly on $q$. As expected, the low-frequency, incoherent mode plotted in Fig. 9 lies much below the SW gap. For small $cq/T_{\rm N}^\star$ and $T=0$ but $z_0\gg 8\sqrt{2}\Delta(0)\phi(0)$,

$$\omega_{\rm i}^{(1)}(\mathbf{q})\approx\frac{\Delta_{\rm sw}(0)^2}{z_0}+\frac{4(cq)^2}{z_0}\left[1-2\left(\frac{z_0}{4\Delta(0)}\right)^2\right] \quad (55)$$

has a quadratic dispersion even when $\Delta_{\rm sw}(0)=0$. But in the limit $z_0\to 0$, $\omega_{\rm i}^{(1)}(\mathbf{q})\approx\sqrt{\Delta_{\rm sw}(0)^2/2+(cq)^2}$ at $T=0$ so that $\omega_{\rm i}^{(1)}(\mathbf{q})$ has a linear dispersion with the same velocity as the SW modes.

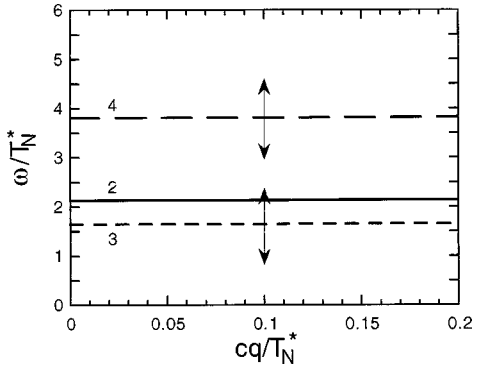


FIG. 8. The dispersion of the incoherent, high-frequency collective modes 2, 3, and 4 for the same parameters as in Fig. 5 with $\kappa/T_{\rm N}^\star=2.5\times10^{-5}$. Also shown are the widths of modes 3 and 4.

Also indicated in Fig. 8 are the broad widths of modes 3 and 4, which are heavily damped. Consequently, these modes will be difficult to observe using neutrons. By contrast, modes 1 and 2 have very narrow peaks that should appear as sharp features in a neutron-scattering cross section. As $T\to 0$, $F_{\rm i}^{(2)}(\mathbf{q}=0,\omega=z_0/2)\to 0$ and mode 2 becomes undamped for small enough $cq$. The first incoherent mode plotted in Fig. 9 also has a very narrow width which vanishes as $T\to 0$ for small $cq$. But like the SW modes, modes 1 and 2 may be additionally damped by impurity scattering or by single-particle excitations of the nongapped portions of the Fermi surfaces. Mode 2 may also be broadened by the variation in energy mismatch $z_0$ around the hole Fermi surface.

The high-frequency, incoherent modes plotted in Fig. 8 are associated with the internal degrees of freedom of the MSDW state. While a SW mode with $\mathbf{q}=0$ corresponds to the uniform rotation of each spin $\mathbf{S}_i$ by the same angle, a high-frequency incoherent mode with $\mathbf{q}=0$ corresponds to the separate rotation of each spin by a different angle. This out-of-phase motion is achieved by the incoherent oscillation of the two or three SDW components $\hat{\mathbf{r}}_\gamma\cos(\mathbf{Q}_\gamma\cdot\mathbf{R}_i)$ in Eqs. (1b) and (1c). Due to the tilting of the spins away from the crystal axis, these incoherent excitations possess both transverse and longitudinal components.

One such high-frequency, incoherent mode may have been observed below the Néel temperature $T_{\rm N}=240$ K of USb,[26] where a TSDW phase was conjectured and modeled

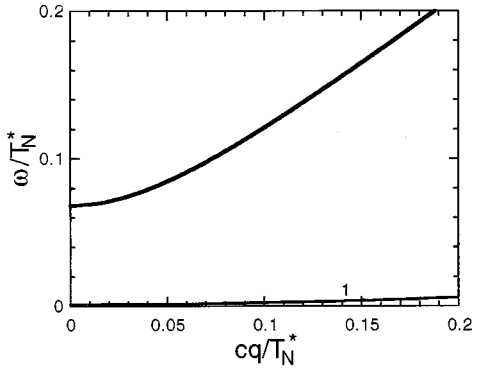


FIG. 9. The dispersion of the low-frequency incoherent mode 1 (thin solid) together with the SW mode (thick solid) for the same parameters as in Fig. 8.

by Jensen and Bak.[27] Starting with an anisotropic Heisenberg model, Jensen and Bak conclude that a high-frequency collective mode with $\omega_i \approx 30$ meV is supported by the internal degrees of freedom of the TSDW structure. Similar conclusions were latter reached by Long and Yeung,[41] also based on a Heisenberg model. However, Hälg *et al.*[42] have argued that multiple domains of an SSDW can explain the appearance of high-frequency magnetic excitations in uranium monopnictides such as USb.

The mathematical origin of the Goldstone mode $\omega_i^{(1)}(\mathbf{q})$ plotted in Fig. 9 can be traced to Eq. (A11) for $\chi_4(\mathbf{q},\omega)$. When $\phi=0$, the condition $1-U\chi_4(\mathbf{q}=0,\omega_i^{(1)}=0)=0$ is equivalent to the self-consistent relation for $\Delta$ given by Eq. (26). Physically, this Goldstone mode corresponds to the dispersion of an unpaired hole, suitably modified to account for its interaction with the condensed electrons. Since unpaired holes only exist in a MSDW state, the Goldstone mode does not appear in the SSDW phase.

## VII. DISCUSSION AND CONCLUSION

This paper has evaluated the magnetic excitations about the S, D, and T SDW states which appear in MnNi, MnCu, and FeMn alloys. When the magnetoelastic coupling is absent, the free energy is invariant under the rotation of every spin $\mathbf{S}_i$ by the same angle. Consequently, the SW excitations are Goldstone modes of the alloy when $\kappa=0$. But when $\kappa>0$, the magnetoelastic interaction generates an effective field $\mathbf{B}_i$, which destroys the rotational invariance of the Hamiltonian and generates a SW gap. A MF description of the magnetoelastic interaction together with an itinerant description of the *d*-band electrons produces the relation $\Delta_{sw}(T)\propto M(T)^{3/2}$, which becomes exact as $M(T)\to 0$. By contrast, a 3/2 power law cannot be obtained from a local-moment description of $\gamma$-Mn alloys based on a Heisenberg model.

In addition to SW excitations, the MSDW states support an additional class of incoherent collective excitations, three of which have high frequencies of order $\Delta(0)\approx 1$ eV. Unfortunately, modes 3 and 4 may be impossible to detect due to their broad widths. Although weakly damped, mode 1 probably lies at too low a frequency to be easily studied using neutrons. By contrast, mode 2 has a very sharp low-temperature peak at $\omega\approx z_0/2<2\Delta(0)$. With increasing temperature, $\omega_i^{(2)}(T,\mathbf{q}=0)$ is predicted to decrease like $M(T)^2 \propto 1-T/T_N$. So above about $0.75T_N\approx 320$ K, the frequency of mode 2 should be in the right range to observe with a modern spallation source. Although the frequency of each incoherent mode is identical in the D and T SDW phases, the prefactors in Eq. (52) indicate that the incoherent mode intensity will be 33% larger in the TSDW phase. Hence, it would be interesting to study the change in intensity of mode 2 as the temperature falls through the fcc (TSDW) to fct (DSDW) transition[4] in $Mn_{1-x}Ni_x$ alloys with $0.18<x<0.22$. The observation of this incoherent mode would also remove the remaining doubt[43] that the cubic phase supports a TSDW state.

Compared to the SSDW state, the intensity of the SW modes in the D and T SDW states is 1/2 and 1/3 times smaller. But the DSDW phase has twice as many magnetic satellites as the SSDW state (the $2N$ *X* points obtained by translating each $\Gamma$ by $\mathbf{Q}_x$ and $\mathbf{Q}_y$) while the TSDW has 3 times as many satellites (all $3N$ *X* points). Hence, the total SW intensity at all of the magnetic satellites is unchanged in the three phases. Since the SW gap only depends on $\kappa$ and $M(T)$, it is not expected to change across a phase transition between different SDW states.

As the temperature approaches $T_N$, $\chi_2\to 0$ and $\chi_3\to\chi_4$ so that $F_{\pm}(\mathbf{q},\omega)\to F_i(\mathbf{q},\omega)$. Consequently, the incoherent and coherent scattering become equal at $T_N$. Inspection of Eqs. (52) and (53) then reveals that the inelastic scattering about every *X* point will be *identical* at the Néel temperature of each SDW phase.

Sandwiched between the S and D SDW phases of MnNi alloys in Fig. 1 lies an orthorhombic phase[4] with $c>b>a$. We are aware of no experimental studies on the spin dynamics of this phase. Even the static spin configuration is in some doubt. Long and Yeung[44] have speculated that the orthorhombic phase is associated with the spin ordering

$$\mathbf{S}_i = M[\hat{z}\cos(\mathbf{Q}_z\cdot\mathbf{R}_i)\cos\theta+\hat{x}\cos(\mathbf{Q}_x\cdot\mathbf{R}_i)\sin\theta], \quad (56)$$

which smoothly interpolates between S and D SDW phases as $\theta$ varies from 0 to $\pi/4$. Unfortunately, this SDW phase cannot be stabilized within our approach because the resulting effective field $\mathbf{B}_i$ of Eq. (11) is not parallel to $\mathbf{S}_i$. Only when $\theta=0$ or $\pi/4$ is the spin configuration stabilized by the magnetoelastic interaction of Eq. (5). However, a more complex magnetoelastic interaction with higher-order terms might be able to stabilize the proposed spin configuration of the orthorombic phase. An alternative SDW configuration was proposed[14] for the orthorhombic phase of MnGa alloys.

This work leaves several other important questions unresolved. Jankowska-Kisielinska *et al.*[23] recently reported that the SW velocity *c* of a fct MnNi alloy is proportional to $M(T)$ at low temperatures. Closer to $T_N$, *c* was observed to become constant. While a linear dependence of $c\propto M(T)$ was predicted by Sato and Maki,[39] our model predicts that *c* is a temperature-independent constant determined by the Fermi surface topology and by the angle between $\mathbf{q}$ and $\mathbf{Q}_\gamma$. Possibly, the observed temperature dependence of *c* is caused by the change in the single-particle background, which grows as the temperature increases.

Throughout this paper, we have assumed that the magnetic moment *M* on each lattice site is the same. So the spin configurations of the various SDW states average over the Mn and impurity moments. This assumption may be expected to fail as the concentration of impurity atoms increases, especially in MnCu alloys where the Cu atoms are nonmagnetic. The tilting of the Mn moments away from the *c* axis in MnCu alloys[13] may be due to the absence of Cu moments. In FeMn alloys, the Mn moment was believed[3] to exceed the Fe moment in both the SSDW and TSDW phases. But recent first-principles calculations by Schulthess *et al.*[45] indicate that for a cubic $Fe_{0.5}Mn_{0.5}$ alloy, the TSDW ground state contains an Fe moment of $2.05\mu_B$ and a smaller Mn moment of $1.91\mu_B$. As shown below, the differences between the Mn, Ni, and Fe moments may have important consequences for the martensitic transformation of MnNi and FeMn alloys.

Within our model, the stable magnetic phase possesses the largest value for $\kappa$. Unfortunately, realistic parameters

for $c_{11}$ and $c_{12}$ imply that the SSDW always has a lower free energy than the MSDW phases. For example, the $Mn_{85}Ni_9C_6$ alloy studied by Lowde *et al.*[31] undergoes a martensitic transformation from fcc to fct phases at $T_m \approx 174$ K, much below the Néel temperature of 546 K. The softening of $c_{11}-c_{12}$ is observed to preceed this transformation. Assuming that the SSDW is somehow eliminated from the competition, then the fcc to fct transition can be qualitatively explained by our model: while $\kappa \propto 1/(c_{11}+2c_{12})$ in the high-temperature TSDW phase, $\kappa \propto 1/(c_{11}-c_{12})$ for a DSDW structure. So the martensitic transformation occurs when $c_{11}-c_{12}$ is small enough that $\kappa(\mathrm{DSDW})=\kappa(\mathrm{TSDW})$. But the measured values for $c_{11}$ and $c_{12}$ imply that the DSDW always has a larger $\kappa$ than the TSDW, even at $T_N$. Moreover, the SSDW has a larger $\kappa$ than either of the MSDW states.

Alloy disorder may explain this behavior. Both Long[46] and Henley[47] have argued that due to the difference between the Mn and Ni moments, doping with Ni impurities stabilizes a noncollinear spin configuration, with the TSDW favored over the DSDW. Henley's magnetic phase diagram for an $XY$ model with randomly vacated sites bears some resemblance to the MnNi phase diagram of Fig. 1. Although the TSDW is favored by disorder for high Ni concentrations, the DSDW may overcome this advantage at low temperatures as $c_{11}-c_{12}$ decreases.

On the other hand, Tsunoda and Wakabayashi[12] have argued that the softening of $c_{11}+2c_{12}$ is responsible for the magnetic and tetragonal phase transitions at $T_m=T_N$ in moderately doped MnCu alloys. Despite the negative value for $c_{12}$, $\kappa$ is still larger for a SSDW than for a DSDW phase. For small impurity concentrations, the DSDW phase may not gain much free energy from random disorder. So our model correctly predicts that the softening of $c_{11}+2c_{12}$ and enhancement of $\kappa$ induce a first-order transition to a tetragonal SSDW phase with $c<a$.

Besides $\gamma$-Mn alloys, the other class of prototypical transition-metal antiferromagnets are Cr alloys. Magnetoelastic interactions are found to be much less significant in Cr than in $\gamma$-Mn. Early measurments by Steinitz *et al.*[48] indicate that the maximum tetragonality $t=1-c/a$ of pure Cr at low temperatures is about $2.5\times10^{-5}$ or roughly 2000 times smaller than in $\gamma$-Mn. Due to its small magnitude, other energies may compete with the magnetoelastic interaction in Cr alloys. Indeed, recent work by Marcus *et al.*[49] suggests that the lattice *expansion* of Cr just below $T_N$ is required to stabilize the SDW. Hence, the tetragonality is negative at high temperatures and only becomes positive below 230 K. So unlike in $\gamma$-Mn, $t$ is not proportional to $M(T)^2$. It is not known if the *change* in $t$ below $T_N$ follows $M(T)^2$.

Despite its tetragonal distortion below $T_N$, Cr shows no signs of a SW gap. Neutron scattering measurments[50] suggest that the largest possible SW gap in pure Cr is 50 $\mu$eV, or about 160 times smaller than in $\gamma$-Mn. As indicated by Eq. (54), the SW gap is proportional to $\sqrt{\kappa}$. Unfortunately, the magnetoelastic constant $\kappa$ cannot be simply related to the tetragonality or volume contraction below $T_N$. Nonetheless, a SW gap of 50 $\mu$eV would imply that $\kappa$ is 25 000 times smaller in Cr than in $\gamma$-Mn.

To summarize, we have studied the spin excitations about the three magnetic phases of $\gamma$-Mn alloys. While a SW mode with energy gap proportional to $M(T)^{3/2}$ is found in all three magnetic states, high-frequency, incoherent modes with frequencies $\omega_i \sim \Delta$ are predicted for the two MSDW states.

## ACKNOWLEDGMENTS

This research was supported by Oak Ridge National Laboratory, which is managed by Lockheed Martin Energy Research Corp. for the U.S. Department of Energy under Contract No. DE-AC05-96OR22464.

## APPENDIX A: SPIN CORRELATION FUNCTIONS

The RPA equations for the spin correlation functions are given by

$$\chi_1=\chi_1^{(0)}+\chi_1^{(0)}U\chi_1+(m-1)\chi_1^{(0)\prime}U\chi_1'+\chi_2^{(0)} \times U[\chi_2+(m-1)\chi_2'], \tag{A1}$$

$$\chi_1'=\chi_1^{(0)\prime}+\chi_1^{(0)}U\chi_1'+\chi_1^{(0)\prime}U(\chi_1+\delta_{m,3}\chi_1') +\chi_2^{(0)}U[\chi_2+(m-1)\chi_2'], \tag{A2}$$

$$\chi_2=\chi_2^{(0)}+\overline{\chi}_1^{(0)}U\chi_2+(m-1)\overline{\chi}_1^{(0)\prime}U\chi_2'+\chi_2^{(0)} \times U[\chi_1+(m-1)\chi_1'], \tag{A3}$$

$$\chi_2'=\chi_2^{(0)}+\overline{\chi}_1^{(0)}U\chi_2'+\overline{\chi}_1^{(0)\prime}U(\chi_2+\delta_{m,3}\chi_2') +\chi_2^{(0)}U[\chi_1+(m-1)\chi_1'], \tag{A4}$$

where $m=1$, 2, or 3 for the S, D, and T SDW phases. These linear, coupled equations are sketched in Fig. 4, where the Coulomb interaction is represented by a wiggly line. A similar set of coupled equations connects $\overline{\chi}_1, \overline{\chi}_1', \overline{\chi}_2$, and $\overline{\chi}_2'$.

The HF correlation functions

$$\chi_1^{(0)}(\mathbf{q},i\omega_n)=-\frac{T}{V}\sum_{l,\mathbf{k}} G(\mathbf{k},i\nu_l)_{aa}G(\mathbf{k}+\mathbf{q},i\nu_l-i\omega_n)_{bb}, \tag{A5}$$

$$\chi_1^{(0)\prime}(\mathbf{q},i\omega_n)=-\frac{T}{V}\sum_{l,\mathbf{k}} G(\mathbf{k},i\nu_l)_{aa}G(\mathbf{k}+\mathbf{q},i\nu_l-i\omega_n)_{bb'}, \tag{A6}$$

$$\overline{\chi}_1^{(0)}(\mathbf{q},i\omega_n)=-\frac{T}{V}\sum_{l,\mathbf{k}} G(\mathbf{k},i\nu_l)_{bb}G(\mathbf{k}+\mathbf{q},i\nu_l-i\omega_n)_{aa}, \tag{A7}$$

$$\overline{\chi}_1^{(0)\prime}(\mathbf{q},i\omega_n)=-\frac{T}{V}\sum_{l,\mathbf{k}} G(\mathbf{k},i\nu_l)_{bb'}G(\mathbf{k}+\mathbf{q},i\nu_l-i\omega_n)_{aa}, \tag{A8}$$

$$\chi_2^{(0)}(\mathbf{q},i\omega_n)=-\frac{T}{V}\sum_{l,\mathbf{k}} G(\mathbf{k},i\nu_l)_{ab}G(\mathbf{k}+\mathbf{q},i\nu_l-i\omega_n)_{ab} \tag{A9}$$

are evaluated with $U=0$. It can be easily shown that $\chi_2^{(0)'}=\overline{\chi}_2^{(0)'}=\overline{\chi}_2^{(0)}=\chi_2^{(0)}$. Notice that $\overline{\chi}_i^{(0)}(\mathbf{q},i\omega_n)=\chi_i^{(0)}(-\mathbf{q},-i\omega_n)$. For convenience, we also introduce the HF susceptibilities

$$\chi_3^{(0)}(\mathbf{q},i\omega_n)=\chi_1^{(0)}(\mathbf{q},\omega)+(m-1)\chi_1^{(0)'}(\mathbf{q},\omega)$$
$$=-\frac{T}{V}\sum_{l,\mathbf{k}} G(\mathbf{k},i\nu_l)_{aa}\frac{i(\nu_l-\omega_n)-\epsilon_a(\mathbf{k}+\mathbf{q})}{D(\mathbf{k}+\mathbf{q},i(\nu_l-\omega_n))}, \tag{A10}$$

$$\chi_4^{(0)}(\mathbf{q},i\omega_n)=\chi_1^{(0)}(\mathbf{q},\omega)-\chi_1^{(0)'}(\mathbf{q},\omega)$$
$$=-\frac{T}{V}\sum_{l,\mathbf{k}} G(\mathbf{k},i\nu_l)_{aa}\frac{1}{i(\nu_l-\omega_n)-\epsilon_{b+}(\mathbf{k}+\mathbf{q})}, \tag{A11}$$

and the corresponding overbarred quantities $\overline{\chi}_3^{(0)}(\mathbf{q},i\omega_n)$ and $\overline{\chi}_4^{(0)}(\mathbf{q},i\omega_n)$.

## APPENDIX B: SPIN-WAVE GAP

Recall that the SW excitations are given by the zeros of the function $F_-(\mathbf{q},\omega)$. To obtain the SW gap at $\mathbf{q}=0$, we separate $F_\pm(\mathbf{q},\omega)$ into real and imaginary parts:

$$F_\pm(\mathbf{q},\omega)=F_\pm^{(1)}(\mathbf{q},\omega)+iF_\pm^{(2)}(\mathbf{q},\omega). \tag{B1}$$

Using the results of Ref. 37 and the modified self-consistent equation for $M(T)$ including magnetoelastic effects, we find

$$F_\pm^{(1)}(\mathbf{q},0)=\frac{1}{2}\rho_{eh}U\phi(T)^2$$
$$+\frac{\pi}{4}iT\rho_{eh}U(\xi^2+2\Delta^2\pm 2\Delta^2)\sum_l\frac{\mathrm{sgn}(\nu_l)}{x_l(x_l^2-\xi^2)}, \tag{B2}$$

$$F_\pm^{(2)}(\mathbf{q},\omega)=U\frac{\pi}{32}\rho_{eh}\{\Theta(\xi^2-\omega^2)+\Theta(\omega^2-4\Delta^2-\xi^2)\}$$
$$\times\left(\frac{\omega^2-4\Delta^2-\xi^2}{\omega^2-\xi^2}\right)^{\pm 1/2}$$
$$\{f[v(\omega)+z_0/4]-f[v(\omega)-\omega+z_0/4]-f[-v(\omega)+z_0/4]$$
$$+f[-v(\omega)+\omega+z_0/4]\}, \tag{B3}$$

where $f(x)=1/[\exp(x\beta)+1]$ is the Fermi function, $\Theta(x)$ is the step function, $\phi(T)$ is defined by Eq. (38), $x_l$ is defined by Eq. (35), and

$$v(x)=\frac{x}{2}+\frac{\xi}{2}\sqrt{\frac{x^2-4\Delta^2-\xi^2}{x^2-\xi^2}}. \tag{B4}$$

The frequency dependence of $F_\pm^{(1)}(\mathbf{q},\omega)$ is extracted using the Kramers-Kronig relation

$$F_\pm^{(1)}(\mathbf{q},\omega)-F_\pm^{(1)}(\mathbf{q},0)=\frac{\omega}{\pi}\int_{-\infty}^{\infty}\frac{d\omega'}{\omega'}\frac{1}{\omega'-\omega}F_\pm^{(2)}(\mathbf{q},\omega'). \tag{B5}$$

With $\mathbf{q}$ measured from $\mathbf{Q}_\gamma$, $\xi=cq$ is simply related to the SW velocity $c$. For octagonal Fermi surfaces with $\mathbf{q}$ parallel to $\mathbf{Q}_\gamma$ or spherical Fermi surfaces with any $\mathbf{q}$, $\xi=v_Fq/\sqrt{3}$. But for cubic Fermi surfaces with $\mathbf{q}$ parallel to $\mathbf{Q}_\gamma$, $\xi=v_Fq$. So the precise value of $c/v_F$ depends on the Fermi surface topology and on the angle between $\mathbf{q}$ and $\mathbf{Q}_\gamma$.

The solution for the SW gap $\omega=\Delta_{\mathrm{sw}}$ with $\xi=0$ is given by the condition

$$-\frac{\omega^2}{4}I_1(\omega)=\phi(T)^2, \tag{B6}$$

$$I_1(\omega)=\int_{2\Delta}^{\infty}\frac{dx}{x^2-\omega^2}\frac{1}{\sqrt{x^2-4\Delta^2}}$$
$$\times\{f(x/2+z_0/4)-f(-x/2+z_0/4)\}. \tag{B7}$$

Complex analysis may be used to show that

$$I_1(\omega)=\frac{\pi}{2\omega}\frac{1}{\sqrt{4\Delta^2-\omega^2}}\{f(\omega/2+z_0/4)-f(-\omega/2+z_0/4)\}$$
$$+\frac{\pi}{2}T\sum_{l=0}^{\infty}\mathrm{Re}\left\{\frac{1}{(\nu_l+iz_0/4)^2+\omega^2/4}\right.$$
$$\left.\times\frac{1}{\sqrt{(\nu_l+iz_0/4)^2+\Delta^2}}\right\}. \tag{B8}$$

Evaluating this expression for small $\omega$ and $\Delta$ with $\omega/\Delta\ll 1$, we obtain Eq. (54) for the SW gap near $T_N$.

## APPENDIX C: INCOHERENT COLLECTIVE MODES

The incoherent collective modes appear only in the D and T SDW states as the zeros of $F_{\mathrm{i}}^{(1)}(\mathbf{q},\omega)$ or $\overline{F}_{\mathrm{i}}^{(1)}(\mathbf{q},\omega)=F_{\mathrm{i}}^{(1)}(\mathbf{q},-\omega)$, which are the real parts of the functions $F_{\mathrm{i}}(\mathbf{q},\omega)=F_{\mathrm{i}}^{(1)}(\mathbf{q},\omega)+iF_{\mathrm{i}}^{(2)}(\mathbf{q},\omega)$ or $\overline{F}_{\mathrm{i}}(\mathbf{q},\omega)=F_{\mathrm{i}}(\mathbf{q},-\omega)^*$. Employing the formalism of Ref. 37, we find

$$F_{\mathrm{i}}^{(1)}(\mathbf{q},0)=\frac{1}{2}\rho_{eh}U\phi(T)^2+\frac{\pi}{4}iT\rho_{eh}U\xi^2$$
$$\times\sum_l\frac{\mathrm{sgn}(\nu_l)}{x_l[(i\nu_l-x_l/2-z_0/4)^2-\xi^2]}, \tag{C1}$$

$$F_{\mathrm{i}}^{(2)}(\mathbf{q},\omega)=U\frac{\pi}{32}\rho_{eh}\{f[r_+(\omega)+z_0/4]-f[r_+(\omega)-\omega+z_0/4]$$
$$+f[r_-(\omega)+z_0/4]-f[r_-(\omega)-\omega+z_0/4]\}, \tag{C2}$$

with

$$r_\pm(\omega)=\frac{1}{2}(\omega\pm\xi)+\frac{1}{2}\frac{\Delta^2}{\omega\pm\xi}. \tag{C3}$$

The frequency dependence of $F_i^{(1)}(\mathbf{q},\omega)$ is obtained from a Kramers-Kronig relation like Eq. (B5).

At $T=0$, it is easy to show that the incoherent mode frequencies with $\xi=0$ and $\omega>0$ are given by

$$\omega_i^{(1)}(\xi=0)=-\frac{z_0}{4}+\frac{1}{2}\sqrt{z_0^2/4+4\Delta(0)^2\{1-\exp[-8\phi(0)^2]\}}, \tag{C4}$$

$$\omega_i^{(2)}(\xi=0)=\frac{z_0}{4}+\frac{1}{2}\sqrt{z_0^2/4+4\Delta(0)^2\{1-\exp[-8\phi(0)^2]\}}, \tag{C5}$$

$$\omega_i^{(3)}(\xi=0)=-\frac{z_0}{4}+\frac{1}{2}\sqrt{z_0^2/4+4\Delta(0)^2\{1+\exp[-8\phi(0)^2]\}}, \tag{C6}$$

$$\omega_i^{(4)}(\xi=0)=\frac{z_0}{4}+\frac{1}{2}\sqrt{z_0^2/4+4\Delta(0)^2\{1+\exp[-8\phi(0)^2]\}}. \tag{C7}$$

Whereas modes 2 and 4 arise from the condition $F_i^{(1)}(\mathbf{q}=0,\omega)=0$, modes 1 and 3 are determined by the condition $\overline{F}_i^{(1)}(\mathbf{q}=0,\omega)=F_i^{(1)}(\mathbf{q}=0,-\omega)=0$.


[1] D. Meneghetti and S. S. Sidhu, Phys. Rev. **105**, 130 (1957).
[2] J. S. Kouvel and J. S. Kasper, J. Phys. Chem. Solids **24**, 529 (1963).
[3] Y. Endoh and Y. Ishikawa, J. Phys. Soc. Jpn. **30**, 1614 (1971).
[4] N. Honda, Y. Tanji, and Y. Nakagawa, J. Phys. Soc. Jpn. **41**, 1931 (1976).
[5] T. Jo and K. Hirai, J. Phys. Soc. Jpn. **55**, 2017 (1986).
[6] T. Takahashi, T. Ukai, and N. Mori, J. Appl. Phys. **63**, 3611 (1988).
[7] S. Fujii, S. Ishida, and S. Asano, J. Phys. Soc. Jpn. **60**, 4300 (1991).
[8] S. J. Kennedy and T. J. Hicks, J. Phys. F **17**, 1599 (1987).
[9] S. Kawarazaki, K. Fujita, K. Yasuda, Y. Sasaki, T. Mizusaki, and A. Hirai, Phys. Rev. Lett. **61**, 471 (1988).
[10] P. Makhurane and P. Gaunt, J. Phys. C **2**, 959 (1969).
[11] N. Cowlam, G. E. Bacon, and L. Gillott, J. Phys. F **7**, L315 (1977).
[12] Y. Tsunoda and N. Wakabayashi, J. Phys. Soc. Jpn. **50**, 3341 (1981).
[13] Y. Tsunoda and Y. Nakai, Solid State Commun. **34**, 413 (1980).
[14] T. Hori, Y. Morii, S. Funahashi, H. Niida, M. Akimitsu, and Y. Nakagawa, Physica B **213&214**, 354 (1995).
[15] K. Mikke, J. Jankowska, and E. Jaworska, Physica B **120B**, 156 (1983).
[16] M. C. K. Wiltshire, M. M. Elcombe, and C. J. Howard, J. Phys. F **15**, 1595 (1985).
[17] J. A. Fernandez-Baca, M. E. Hagen, R. M. Nicklow, Y. Tsunoda, and S. M. Hayden, J. Magn. Magn. Mater. **104-107**, 699 (1992); J. A. Fernandez-Baca, M. E. Hagen, R. M. Nicklow, T. G. Perring, and Y. Tsunoda, J. Appl. Phys. **73**, 6548 (1993).
[18] K. Mikke, T. M. Holden, J. A. Fernandez-Baca, E. Fawcett, and J. Jankowska-Kiseilińska, in *Physics of Transition Metals*, edited by P. M. Oppeneer and J. Kubler (World Scientific, Singapore, 1993), Vol. II, p. 659.
[19] Jankowska-Kiseilińska, E. Jaworska, K. Mikke, and J. J. Milczarek, in *Physics of Transition Metals*, edited by P. M. Oppeneer and J. Kubler (World Scientific, Singapore, 1993), Vol. II, p. 655.
[20] Y. Endoh, G. Shirane, Y. Ishikawa, and K. Tajima, Solid State Commun. **13**, 1179 (1973).
[21] K. Tajima, Y. Ishikawa, Y. Endoh, and Y. Noda, J. Phys. Soc. Jpn. **41**, 1195 (1976).
[22] K. Mikke, J. Jankowska-Kisienlinska, and E. Jaworska, Physica B **180&181**, 247 (1992).
[23] J. Jankowska-Kisielinska, K. Mikke, and J. J. Milczarek, J. Phys.: Condens. Matter **9**, 10 761 (1997).
[24] J. Yamashita, S. Asano, and S. Wakoh, J. Appl. Phys. **39**, 1274 (1968).
[25] P. A. Fedders and P. C. Martin, Phys. Rev. **143**, 245 (1966).
[26] G. H. Lander and W. G. Stirling, Phys. Rev. B **21**, 436 (1980).
[27] J. Jensen and P. Bak, Phys. Rev. B **23**, 6180 (1981).
[28] R. S. Fishman and S. H. Liu, Phys. Rev. B **58**, 5912 (1998).
[29] These are sometimes refered to as single, double, and triple $Q$ states.
[30] R. S. Fishman, X. W. Jiang, and S. H. Liu, Phys. Rev. B **58**, 414 (1998).
[31] R. D. Lowde, R. T. Harley, G. A. Saunders, M. Sato, R. Scherm, and C. Underhill, Proc. R. Soc. London, Ser. A **374**, 87 (1981).
[32] In Ref. 28, $\rho_{eh}$ was defined as the density of states for a pair of nested electron and hole Fermi surfaces.
[33] S. Asano and J. Yamashita, J. Phys. Soc. Jpn. **31**, 1000 (1971).
[34] Both $2\Delta(0)$ and $T_N^\star$ were severely underestimated in Ref. 28.
[35] R. S. Fishman and S. H. Liu, Phys. Rev. B **48**, 3820 (1993).
[36] We have modified the conventions for the susceptibilities so that the functions $F_-(\mathbf{q},\omega)$ and $F_i(\mathbf{q},\omega)$ are identical to the functions $1-U[\chi_1(\mathbf{q},\omega)-m\chi_2(\mathbf{q},\omega)]$ and $1-U\chi_3(\mathbf{q},\omega)$ defined in Ref. 28. While $\chi_2(\mathbf{q},\omega)$ is the same in both papers, the susceptibilities $\chi_3(\mathbf{q},\omega)$ and $\chi_4(\mathbf{q},\omega)$ used here are the same as $\chi_1(\mathbf{q},\omega)$ and $\chi_3(\mathbf{q},\omega)$ from our previous paper.
[37] R. S. Fishman and S. H. Liu, Phys. Rev. B **54**, 7233 (1996).
[38] M. J. Gillan, J. Phys. F **3**, 1874 (1973).
[39] H. Sato and K. Maki, Prog. Theor. Phys. **55**, 319 (1976).
[40] See, for example, K. Yosida, *Theory of Magnetism* (Springer, Berlin, 1991).
[41] M. W. Long and W. Yeung, J. Phys. C **19**, 1409 (1986).
[42] B. Hälg, A. Furrer, J. K. Kjems, and O. Vogt, Phys. Rev. Lett. **50**, 1085 (1983).
[43] P. Bisanti, G. Mazzone, and F. Sacchetti, J. Phys. F **17**, 1425 (1987).
[44] M. W. Long and W. Yeung, J. Phys. F **17**, 1195 (1987).

[45] T. C. Schulthess, W. H. Butler, G. M. Stocks, S. Maat, and G. J. Mankey (unpublished).
[46] M. W. Long, J. Phys.: Condens. Matter **1**, 2857 (1989).
[47] C. L. Henley, Phys. Rev. Lett. **62**, 2056 (1989).
[48] M. O. Steinitz, L. H. Schwartz, J. A. Marcus, E. Fawcett, and W. A. Reed, Phys. Rev. Lett. **23**, 979 (1969).
[49] P. M. Marcus, S.-L. Qiu, and V. L. Moruzzi, J. Phys.: Condens. Matter **10**, 6541 (1998).
[50] B. H. Grier, G. Shirane, and S. A. Werner, Phys. Rev. B **31**, 2892 (1985).